

## FIRST-PRINCIPLES INVESTIGATION OF STRUCTURAL AND ELECTRONIC PROPERTIES AND SPIN POLARIZABILITY OF $\text{Cu}_{(3-x)}\text{Mn}_x\text{Al}$ ( $x = 0, 1$ ) INTERMETALLIC COMPOUNDS

Intermetallic compounds (IMCs) including transition metals and p-block metals exhibit high resistance to corrosion and oxidation, low density, high conductivity, and magnetic polarizability. In this study, the first-principles calculations method based on Density Functional Theory (DFT) has been used to investigate the structural and electronic properties, charge density distribution, spin polarizability, and magnetic behavior of  $\text{Cu}_{(3-x)}\text{Mn}_x\text{Al}$  ( $x = 0, 1$ ) intermetallic compounds. Generalized Gradient Approximation (GGA) was employed with Perdew-Burke-Ernzerhof (PBE) exchange-correlation. Calculation of metallic and conductive nature and structural properties was performed simultaneously for all crystal lattices of  $\text{Cu}_{(3-x)}\text{Mn}_x\text{Al}$  ( $L1_2$ ,  $D0_3$ , and Heusler  $L2_1$ ) with  $221\text{-Pm}3m$ ,  $225\text{-Fm}3m$  space groups. Notably, the study clarifies the stoichiometric similarity and difference between  $L1_2$  and  $D0_3$  type structures by presenting a detailed discussion of the  $D0_3$  structure and its targeted properties for the first time. The lattice constant values obtained by performing various optimizations are in excellent agreement with previously reported experimental and theoretical data. The electron density distribution and population analysis are consistent and reveal the dominant bonding type in each IMC. Furthermore, Spin Polarizability analysis has been carried out to demonstrate the magnetic nature of the  $\text{Cu}_2\text{MnAl}$  ( $L2_1$ ) Full Heusler alloy upon the addition of the Mn atom.

**Keywords:** Cu-Al intermetallic; Density Functional Theory (DFT); Structural analysis, Electronic properties, Bonding nature, Spin polarizability

### 1. Introduction

Over the past two decades, the increasing demand for structural materials capable of withstanding severe oxidizing environments and high operating temperatures has led to extensive research on the feasibility of intermetallic compounds [1]. The compounds including transition metals and p-block metals, e.g. Aluminum, have garnered attention due to their relatively low density, high resistance to corrosion and oxidation, high melting points, elevated temperature strength, and high conductivity, making them suitable candidates for high-temperature structural applications [2,3].

Among these compounds, Cu-Al [4], with different structure types, has been widely investigated. Cu-Al-based intermetallic compounds (IMCs) are extensively used in various industries, including electrical, light, aircraft, machinery manufacturing, and construction, due to their superior mechanical strength and low density compared to pure Al and pure Cu [5]. They also exhibit many promising elastic, electronic, and structural properties,

such as good ductility, high tensile strength, thermal stability, and high corrosion resistance [6].

Cu-Al-based alloys possess various stable configurations, in particular  $\text{Cu}_3\text{Al}$  with  $L1_2$  ( $221\text{-Pm}3m$ ) and  $D0_3$  ( $225\text{-Fm}3m$ ) type structures [7-9] as well as the  $\text{Cu}_2\text{MnAl}$  ternary Heusler alloy [10], [11] with  $L2_1$  type structure. Notably, the Heusler  $L2_1$  type structure is partly different from the  $D0_3$ , despite both of them ( $D0_3$  and  $L2_1$ ) belonging to the cf16 Pearson symbol, and sharing the same space group No. of  $225\text{-Fm}3m$ . The  $L2_1$  features one additional element in the same crystal lattice and can be doped in place of Cu atoms in the unit cell edges in the  $D0_3$  structure type. Doping of binary Cu-Al alloys with Mn reduces the decomposition speed of solid solution under aging and alters the physical and mechanical characteristics of the material [12].  $\text{Cu}_2\text{MnAl}$  is also classified as a notable Heusler alloys [10].

Heusler alloys are ternary intermetallic compounds with conventional composition XYZ (Half-Heusler) and  $X_2YZ$  (Full-Heusler). Since their discovery a century ago, they have attracted significant interest [10,13], mainly due to their versatile magnetic

<sup>1</sup> SAKARYA UNIVERSITY, DEPARTMENT OF NANOSCIENCE AND NANOENGINEERING, INSTITUTE OF NATURAL SCIENCES, 54140, SAKARYA, TÜRKIYE

\* Corresponding author: [marefat.khanghah@ogr.sakarya.edu.tr](mailto:marefat.khanghah@ogr.sakarya.edu.tr)



properties. The unique properties of ferromagnetic Heusler alloys have sparked a significant increase in scientific interest, driven by their potential applications in various technical fields. For instance, the development of spintronic materials relies heavily on ferromagnetic Heusler alloys with full spin polarization at the Fermi level [14-19].

First-principles calculations in the frame of the density-functional theory have in recent years become a significant tool for the accurately studying the mechanical properties and crystalline and electronic structures of solids [20]. Hence, the structural and electronic as well as spin polarizability properties of Cu-Al IMCs and their structural study with space group of  $221-Pm3m$  ( $L1_2$ ) for the  $Cu_3Al$  IMCs have recently been investigated systemically [1,8,21-23]. Using a first-principles method, R. Parvin et al. theoretically investigated the band structure of  $Cu_3Al$  IMCs. However, studies on electronic and spin polarizability properties, particularly for the other structure types of  $Cu_3Al$  IMCs with  $225-Fm3m$  ( $D0_3$ ) are still very limited due to computational complexities and testing method limitations.

A review of the literature reveals that only a few studies have simultaneously reported on different space groups and structure types of  $Cu_3Al$  IMCs, as well as  $Cu_2MnAl$  ternary Heusler [24-26], while the theoretical modeling of these studies has been largely overlooked [4,8,27]. To the best of our knowledge, only a handful of studies have been conducted to simulate the optimized geometry and calculate the structural, electronic, and spin polarizability behavior, specifically for the  $D0_3$  and  $L2_1$  structure types of  $Cu_3Al$  intermetallic compounds, relative to other structure types [8,27]. The studies in question have also focused on a separate set of properties than those focused on in the present study.

In this paper, we present a theoretical model based on first-principles calculations in the frame of Density Functional Theory (DFT) [28,29] using the CASTEP code [30], to study structural, electronic, and polarizability of different phases ( $L1_2$ ,  $D0_3$ , and Heusler  $L2_1$ ), of  $Cu_3Al$  IMCs compounds. The findings demonstrate an agreement between experimental and other theoretical results.

The remaining sections of this study are organized as follows: Section 2 provides a brief overview of the computational details. Section 3 presents the results and discussion, including its subsections. Finally, Section 4 summarizes the conclusions drawn from our study.

## 2. Computational details

All calculations were performed utilizing the pseudo-potential technique based on plane-wave density functional theory (DFT) [28,29] as implemented in Cambridge Serial Total Energy Package (CASTEP) [30] computer program. The generalized gradient approximation (GGA) in the form of Perdew-Burke-Ernzerhof (PBE) was used as the exchange-correlation potential [31]. This program appraises the total energy of periodically (PBC – Periodic Boundary Condition) repeating geometries within the frame of density-functional theory and the pseudo-potential

approximation [28,29,32]. The interaction of the valence-core electrons was represented by Vanderbilt-type ultrasoft pseudopotential [33], while the valence electrons are represented explicitly in the calculations; therefore, the potential of the constituent atoms was estimated under the assuming the neutral atomic configurations of  $3s^2 3p^1$  and  $3d^{10} 4s^1$  as valence electrons for Al and Cu, respectively. The Brillouin zone was sampled using the Monkhorst-Pack scheme [34]. The number of  $k$ -point grids and cutoff energy were increased until the calculated total energy converged within the required tolerance (total energy difference  $<1$  meV). After convergence, the optimal  $k$ -point grids with mesh parameters  $16 \times 16 \times 16$  and plane-wave cutoff energy of 500 eV were chosen to obtain equilibrium lattice parameters and calculate the band structure, and the polarizability properties of  $Cu_3Al$  intermetallic with space group of  $225-Fm3m$  ( $D0_3$ ). For other types of  $Cu_3Al$  intermetallics with the space group  $221-Pm3m$  ( $L1_2$ ),  $k$ -point  $18 \times 18 \times 18$  and a plane-wave cutoff energy of 500 eV were used. The electron wave function was expanded in plane waves up to an energy cutoff of 500 eV and a  $12 \times 12 \times 12$  mesh was employed for sampling the Brillouin zone of the Heusler alloy ( $L2_1$ ).

The structural parameters of  $Cu_3Al$  intermetallics were determined using the Broyden Fletcher Goldfarb Shanno (BFGS) minimization scheme [35] with the following convergence criteria: energy change per atom less than  $10^{-5}$  eV, maximum force less than 0.03 eV/Å, maximum stress below 0.05 GPa, maximum displacement of atoms less than  $1.0 \times 10^{-3}$  Å and self-consistent field tolerance during the geometry optimization fixed to  $1.0 \times 10^{-6}$  eV/atom.

## 3. Results and discussion

### 3.1. Geometric Optimization & Structural Properties

$Cu_{(3-x)}Mn_xAl$  ( $x = 0, 1$ ) IMCs for  $x = 0$  crystallize into two cubic  $Cu_3Al$  ( $Cu_3Al$  compound) prototype structures, referred to as  $L1_2$  and  $D0_3$  [7-9]. The first type structure of  $Cu_3Al$  is  $L1_2$  with space group  $Pm-3m$  (No. 221), consisting of Al atoms at the corners and Cu atoms at the face centers of the cube, and can be defined by Wyckoff positions: Al @ 1a (0, 0, 0) and Cu @ 3c (0, 1/2, 1/2). The second structure,  $D0_3$ , has a space group of  $Fm-3m$  (No. 225) and consists of Al atoms at the corners and Cu atoms at the edges of the cube and inside the cell, which can be defined by Wyckoff positions: Al @ 4a (0, 0, 0), Cu @ 4b (1/2, 1/2, 1/2) & 8c (1/4, 1/4, 1/4).

The ternary ordered  $Cu_2MnAl$  (For  $x = 1$ ) Heusler alloy (space group No. 225:  $Fm-3m$ ), in which Al atoms occupy the 4a Wyckoff positions (0,0,0), Cu atoms occupy the 8c site (1/4,1/4,1/4) and Mn atoms occupy the 4b site (1/2,1/2,1/2). From a structural point of view, the Heusler family can be categorized into two types: Full-Heusler  $X_2YZ$  phases where X and Y belong to the transition metal elements and Z is the main group s-p element (p-block) [13,36]. This type structures typically crystallize in the  $Cu_2MnAl$  ( $L2_1$ ) type structure, and the Half-Heusler  $XYZ$  phases with  $C1_b$  structure. In Full-Heusler alloys, the  $Cu_2MnAl$ -

type is obtained when the X atom is more electronegative than Y, and the Hg<sub>2</sub>CuTi-type is obtained when the valance electron of Y atom is larger than X. To date, numerous Ti<sub>2</sub>, Sc<sub>2</sub>, and Mn<sub>2</sub> – Heusler alloys with the Hg<sub>2</sub>CuTi structure have been reported to exhibit Half-metallic (HM) magnetic behavior or even spin gapless semiconductor properties [37]. The cubic phase atomic occupancies of all Cu<sub>(3-x)</sub>Mn<sub>x</sub>Al (x = 0, 1) IMCs with L1<sub>2</sub>, D0<sub>3</sub>, and Heusler L2<sub>1</sub> type structures are illustrated in Figs. 1(a) and 1(b), and 1(c), respectively.

The optimal lattice constant is the value at which the total energy is minimized [38,39]. To determine the stable optimal value and obtain the equilibrium lattice constant, we calculated the total energy against different lattice constants, and the results are reported in Fig. 2. The data obtained were fitted with a third-ordered cubic polynomial equation, revealing the minimum energy at a lattice constant of  $a_0 = 0.3691$  nm (3.691 Å), 0.5860 nm (5.860 Å), 0.5955 nm (5.955 Å) for L1<sub>2</sub>, D0<sub>3</sub>, and Heusler L2<sub>1</sub>), respectively. As evident from TABLE 1, the lattice constant exhibits excellent agreement with previous theoretical calculations and experimental data [1,8,9,11,40-44].

Furthermore, the volume (lattice parameter<sup>3</sup>) at zero pressure, bulk modulus, and the first derivative of bulk modulus were

obtained by fitting the *pressure (P) – volume (V)* curve with the results presented in TABLE 1. The bulk modulus characterizes a material's ability to resist deformation when subjected to external pressure. For solid materials, the bulk modulus indicates the compressibility of the materials, which is associated with their impact sensitivity [45,46]. A well-known method for characterizing the behavior of solid materials under pressure is the 3<sup>rd</sup>-order Birch-Murnaghan (BM3-EOS) equation (formula (1)) [47,48].

$$P(V) = \frac{3B_0}{2} \left[ \left( \frac{V}{V_0} \right)^{-7/3} - \left( \frac{V}{V_0} \right)^{-5/3} \right] \left\{ 1 + \frac{3}{4}(B' - 4) \left[ \left( \frac{V}{V_0} \right)^{-2/3} \right] - 1 \right\} \quad (1)$$

Where  $P$  is pressure,  $B_0$  is the Bulk modulus,  $V$  is the deformed volume,  $V_0$  is the initial volume, and  $B'$  is the first derivative of the bulk modulus with respect to pressure.

A comparison of our results reveals reasonable agreement with both theoretical and experimental values. All the values determined in this stage are used in the subsequent calculations

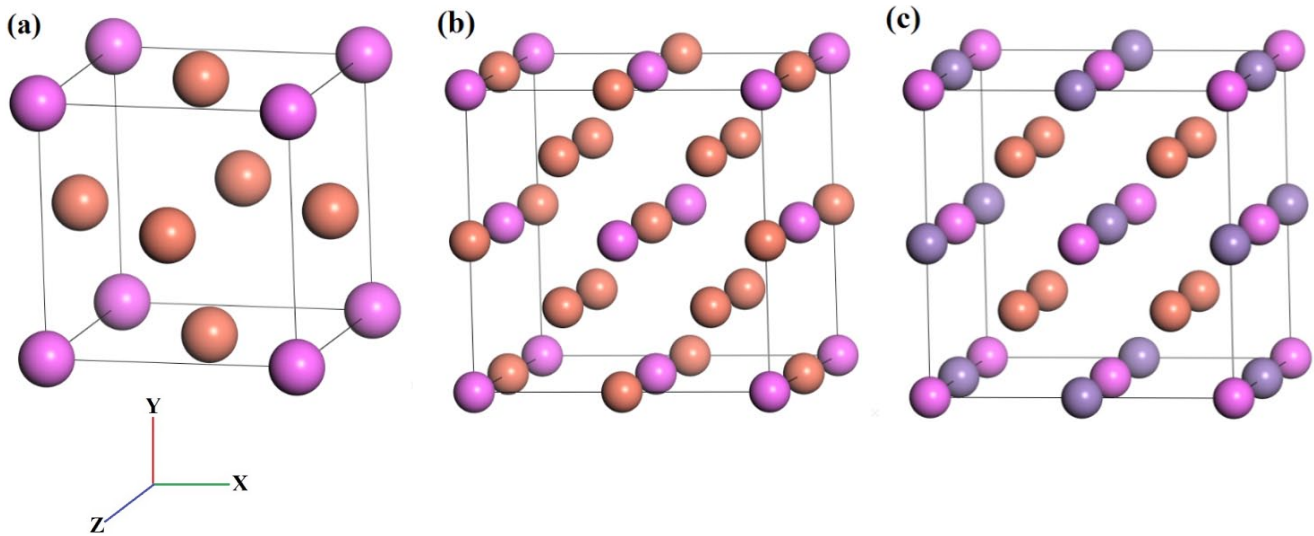


Fig. 1. Cubic phase atomic occupancies of all Cu<sub>(3-x)</sub>Mn<sub>x</sub>Al (x = 0, 1) IMCs with L1<sub>2</sub> (a), D0<sub>3</sub> (b), and Heusler L2<sub>1</sub> (c) type structures. Lilac colors are representative of Al atoms and orange ones represent Cu atoms

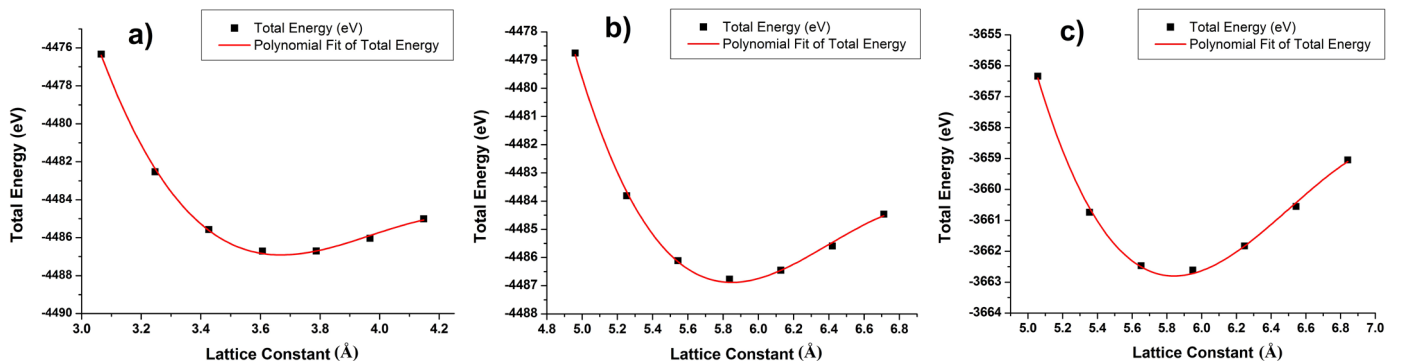


Fig. 2. The total energy of Cu<sub>3</sub>Al IMCs with different crystal structures under different lattice constants. L1<sub>2</sub> (a) type structure. D0<sub>3</sub> (b) type structure. Heusler L2<sub>1</sub> (c) type structure

Calculated lattice parameter ( $a$ ), bulk modulus ( $B$ ), and its pressure derivative ( $B'$ ) for different crystal structures

| Compound             | Type Structure  | References                  | $a$ [Å]           | $B_0$ [GPa]    | $B'$         |
|----------------------|-----------------|-----------------------------|-------------------|----------------|--------------|
| Al                   | FCC-A1          | <b>This work</b>            | <b>4.0488</b>     | <b>76.672</b>  | <b>4.590</b> |
|                      |                 | Calc. [8]                   | 4.05              | 75.937         | 4.588        |
|                      |                 | Exp. [44]                   | 4.0496            | 76.866         | —            |
| Cu                   | FCC-A1          | <b>This work</b>            | <b>3.641</b>      | <b>133.521</b> | <b>4.881</b> |
|                      |                 | Calc. [8]                   | 3.65              | 131.82         | 4.983        |
|                      |                 | Exp. [44]                   | 3.615             | 137.8          | —            |
| Cu <sub>3</sub> Al   | L1 <sub>2</sub> | This work (from Cubic fit)  | 3.669             | —              | —            |
|                      |                 | <b>This work (from EOS)</b> | <b>3.691</b>      | <b>129.205</b> | <b>4.709</b> |
|                      |                 | Calc. [1]                   | —                 | 130.15         | -            |
|                      |                 | Calc. [8]                   | 3.7               | 126.72         | 4.675        |
|                      | D0 <sub>3</sub> | This work (from Cubic fit)  | 5.849             | —              | —            |
|                      |                 | <b>This work (from EOS)</b> | <b>5.860</b>      | <b>129.11</b>  | <b>4.741</b> |
| Cu <sub>2</sub> MnAl | L2 <sub>1</sub> | Calc. [8]                   | 5.877             | 126.23         | 4.117        |
|                      |                 | Exp. [44]                   | 5.83[40] 5.80[41] | —              | —            |
|                      |                 | Exp. [44]                   | —                 | 129.6[8]       | —            |
|                      |                 | This work (from Cubic fit)  | 5.842             | —              | —            |
|                      |                 | <b>This work (from EOS)</b> | <b>5.955</b>      | <b>125.654</b> | <b>4.048</b> |
|                      |                 | Calc. [42]                  | 5.927             | 126.689        | 4.066        |
|                      |                 | Exp. [11]                   | 5.949             | —              | —            |
|                      |                 | Exp. [43]                   | 5.984             | —              | —            |

to enhance convergence, accelerate computation, and ultimately improve the accuracy of the results.

The lattice constant determined for all IMCs in this study exhibits a discrepancy of approximately 2% compared to the experimental value. Furthermore, slight differences are observed between these results and other theoretical values, which can be attributed to the utilization of different calculation methods. These findings highlight the reliability of our current DFT-based first-principles calculations. The observed discrepancy can be attributed to the fact that our calculated data are simulated at 0 Kelvin, whereas the experimental data are obtained at room temperature, which introduces variations in parameters.

### 3.2. Electronic Band Structure & DOS

The spectrum of energy eigenvalues in a periodic system is referred to as the band structure. Band structure calculations provide valuable insights into the form of the Fermi surface.

By analyzing the dominant bands near the Fermi level, their energy status, etc. one can understand the electronic and optical properties of materials. One of the most useful parameters of the band structure is the band gap, which has a profound impact on the optical and electrical properties of the material [49,50]. The electronic band structure of all Cu<sub>(3-x)</sub>Mn<sub>x</sub>Al ( $x = 0, 1$ ) type structures along the high symmetry points (X-R-M-G-R) for L1<sub>2</sub> and (W-L-G-X-Y-K) for D0<sub>3</sub> and Cu<sub>2</sub>MnAl (L2<sub>1</sub>) in the Brillouin zones are presented in Fig. 3(a), (b) and (c), respectively. The band structure of Cu<sub>3</sub>Al IMCs was computed at equilibrium volume (zero pressure,  $P = 0$ ). The Fermi level is set at zero energy value.

Fig. 3(a), (b), and (c) reveal the conductive and metallic nature of both Cu<sub>3</sub>Al IMCs and Cu<sub>2</sub>MnAl due to the overlap of valence and conduction bands at the Fermi level. The band structures of all crystals are reasonably consistent with previous studies. The valence region of L1<sub>2</sub> extends from  $-10.28$  eV up to the Fermi level  $E_F = 0$  eV, and similar trends are observed for other type structures (D0<sub>3</sub>, and Heusler L2<sub>1</sub>). The conduction

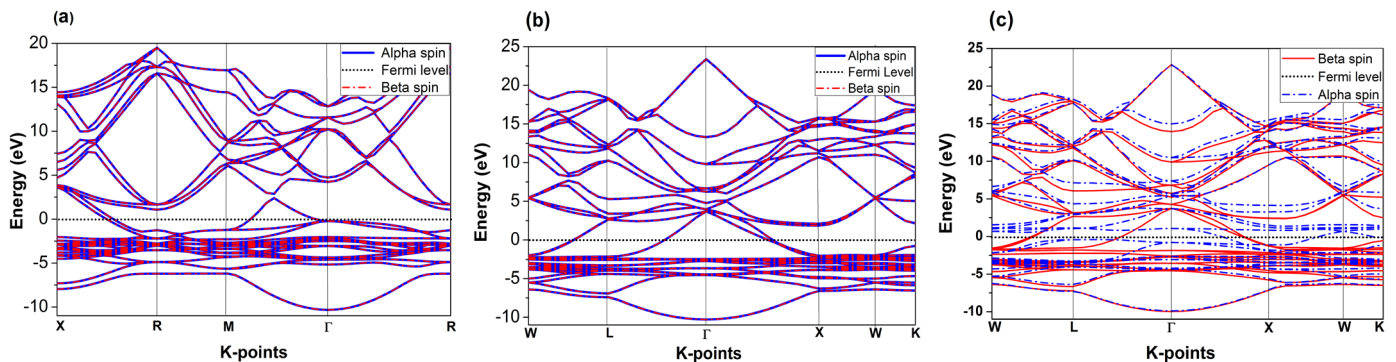


Fig. 3. Calculated band structures of (a) L1<sub>2</sub> type structure; (b) D0<sub>3</sub> type structure; (c) Heusler L2<sub>1</sub> type structure

regions span from the Fermi level  $E_F = 0$  eV up to 18.5 eV and 23.2 eV for  $L1_2$  and both  $D0_3$  and Heusler  $L2_1$  type structures.

From Fig. 3(a) and (b) it is evident that  $L1_2$  and  $D0_3$  type structures exhibit no spin polarizability, as the spin-up (alpha) bands (depicted in blue) coincide with the spin-down (beta) bands (depicted in red), resulting in identical electron paths illustrated on the band structure. In contrast, Fig. 3(c) reveals that for the  $L2_1$  type structure, both up-spin (alpha) and down-spin (beta) electrons originating from Mn atoms follow distinct paths, indicating magnetic and spin polarizability in this structure.

The density of states (DOS) study provides crucial insights into the physical properties of materials. The total density of states (TDOS) and the partial density of states (PDOS) of Cu, Al, and Mn atoms are depicted in Fig. 4(a), (b) and (c). It is evident that all the type structures of  $Cu_{(3-x)}Mn_xAl$  IMCs possess a metallic character, as indicated by the presence of a finite density of states (DOS) at the Fermi level. The fundamental characteristics of these compounds are primarily governed by the d bands of Cu. For  $L1_2$ , in the range of  $-11$  and  $0$  eV, the total density of states is mainly attributed to the  $Cu-3d$  states.

Beyond the Fermi level, the total density of states (TDOS) is predominantly dominated by the  $Cu-p$  and  $Cu-s$  orbitals, with contributions from the  $Al-s$  and  $Al-p$  states. Additionally, a significant hybridization is observed between the  $Al-p$ ,  $Al-s$ ,  $Cu-p$ , and  $Cu-s$  states at energies exceeding  $-2$  eV and below  $-5$  eV. The  $Cu-d$  and  $Al-p$  states exhibit strong hybridization in the range of  $-5$  to  $-3$  eV. The DOS of the  $D0_3$  type structure in Fig. 4(b) is very similar to that of  $L1_2$  (Fig. 4(a)), with the notable difference that the conduction band of  $D0_3$ , extending up to  $+17$  eV, primarily arises from  $Al-s$  and  $p$  states. The strong hybridizations are observed near  $-4$  eV and on  $-2.5$  eV arises from  $Al-p$  and  $Cu-d$  states and arises from  $Al-s$  and  $Cu-p$  states, respectively. Additionally, beyond the Fermi level, Al and Cu states exhibit collective contributions.

The TDOS and PDOS of  $L2_1$  type structure have also been studied as presented in Fig. 4. (c). As evident from Fig. 4(c), there is not any energy gap around the Fermi level, thereby confirming the metallic nature of the  $L2_1$  structure. The lowest valence bands below  $-6$  eV for  $Cu_2MnAl$  are entirely attributed to  $Al-s$  states,

while the bands from  $-5.5$  up to  $3$  eV are predominantly caused by the  $Cu-3d$  and  $Mn-3d$  states.

Our results for the  $L2_1$  type structure exhibit excellent consistency with previously reported studies by B. Benichou et al. [42], Rai et al. [51], and Kulkova et al. [52].

### 3.3. Charge Density Distribution & Population Analysis

Charge Density Distribution is a valuable feature for examining bonding behaviors [53]. Fig 5. presents the charge density distribution maps on the  $(0\ 0\ 1)$  plane for all type structures. The contour lines in Fig. 5(a)  $L1_2$ , (b)  $D0_3$ , (c)  $L2_1$  are plotted from  $0$  to  $1\ e/A^3$  with  $0.2\ e/A^3$  intervals. The region with higher density corresponds to the distribution of core electrons within the atoms, which contributes minimally to bonding. In Fig. 5(a) ( $L1_2$ ), the red color represents the Cu atom, while the nearest neighbors are Al atoms. The charge density distribution maps primarily demonstrate ionic bonding between Cu and Al atoms, resulting from the gain and loss of free electrons. On the other hand, there is an overlap between the orbitals of Al atoms, despite their distance from each other, suggesting covalent Al-Al bonds. In contrast, no such overlap is observed between Cu-Cu atoms, indicating that copper atoms form metallic bonds.

Fig. 5(b) ( $D0_3$ ) also reveals metallic bonding between Cu-Cu atoms, characterized by the absence of orbital overlap and the presence of an electron cloud around them. For Al, it can be inferred that the Al atom exhibits ionic bonding with adjacent Cu atoms and covalent bonding with the farther Cu atoms. Moreover, the overlap between Al-Al atoms is evident, suggesting covalent bonding between them.

In Fig. 5(c) ( $L2_1$ ), metallic bonding between Cu-Cu atoms is also observed. For Al, it can be inferred that the Al atom exhibits covalent bonding with adjacent Cu atoms and is strongly covalent with the Mn atoms. Furthermore, the overlap between Al-Al atoms is evident, suggesting covalent bonding between them. Additionally, Mn-Cu bonding appears to be a combination of ionic and covalent bonding.

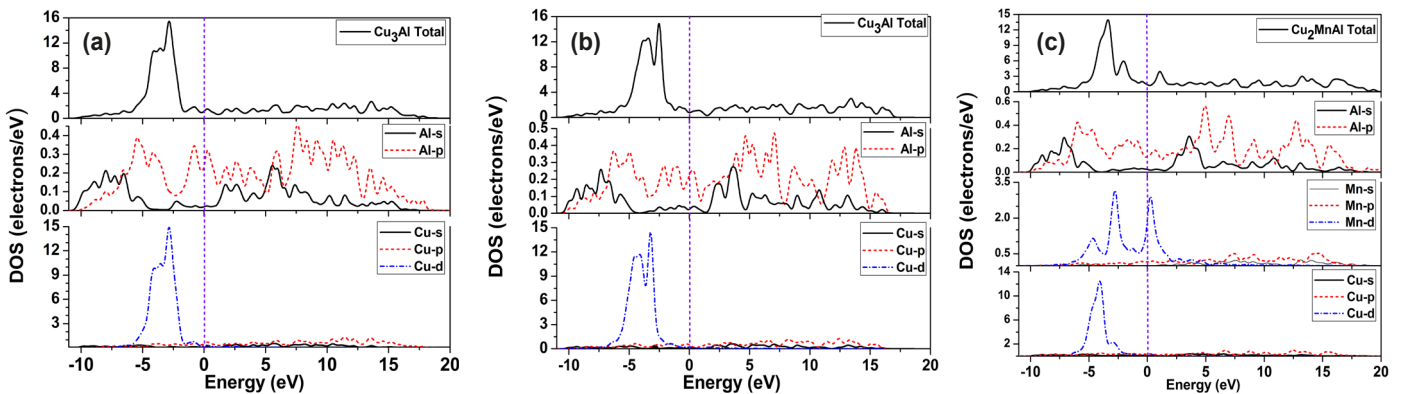


Fig. 4. The total and partial density of states (DOS) of (a)  $L1_2$ , and the Fermi level is set at zero energy and marked by the vertical lines; (b)  $D0_3$ , and the Fermi level is set at zero energy and marked by the vertical lines; (c)  $L2_1$  and the Fermi level is set at zero energy and marked by the vertical lines

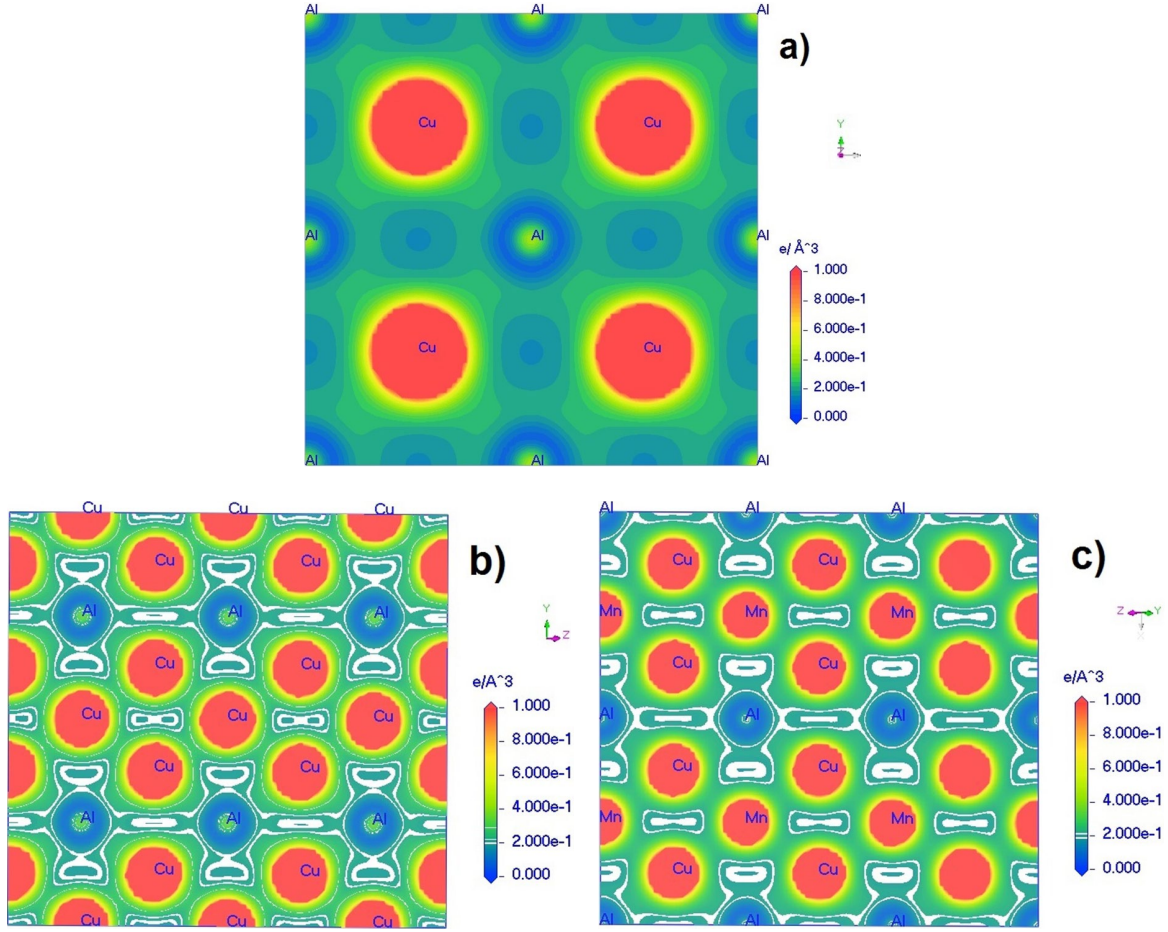


Fig. 5. Contour plot of the electronic charge density in (0 0 1) plane: (a) L1<sub>2</sub>; (b) D0<sub>3</sub>; (c) L2<sub>1</sub>

To gain further insight into the bonding properties of all IMCs, we performed a Mulliken population analysis [54]. This analysis can explain the distribution of electrons in various fractional ways between formed chemical bonds. As observed by Segall et al. [55] there is a strong correlation between covalency [45], bond strength, and ionicity of bonds, which can be quantified by overlap population and Mulliken charge values.

In this analysis, the Mulliken charge  $Q(A)$  of one atom coupled with a particular atom-A (formula (2)), and overlap population  $N(A, B)$  in a typical A-B bond (formula (3)) can be defined as:

$$Q(A) = \sum_k W(k) \sum_v^A P_{\mu\nu}(k) S_{\mu\nu}(k) \quad (2)$$

$$N(A, B) = \sum_k W(k) \sum_{\mu}^A \sum_{\nu}^B P_{\mu\nu}(k) S_{\mu\nu}(k) \quad (3)$$

Where  $P_{\mu\nu}(k)$  and  $S_{\mu\nu}(k)$  are the density matrix and the overlap matrix, respectively.  $\mu$  and  $\nu$  belong to the orbitals of A and B atoms, respectively.  $W(k)$  is the weight associated with the  $k$ -points in the Brillouin zone.

As evident from TABLE 2, electrons are transferred from the Al atom to the Cu atoms in all phases, as indicated by the total

charges of 0.47 and  $-0.48$ , 0.49 and  $-0.48$ , and 0.35 and  $-0.34$  for Al and Cu atoms in L1<sub>2</sub>, D0<sub>3</sub>, L2<sub>1</sub> type structures, respectively. Loss and gain of electrons indicate that charge transfer occurs in Cu<sub>(3-x)</sub>Mn<sub>x</sub>Al, imparting ionic characteristics to these crystals.

The charge transfer in Cu<sub>(3-x)</sub>Mn<sub>x</sub>Al phases is responsible for their ionic nature in chemical bonding, indicating that these crystals exhibit some degree of ionic character.

### 3.4. Spin Polarizability & Magnetic Behavior

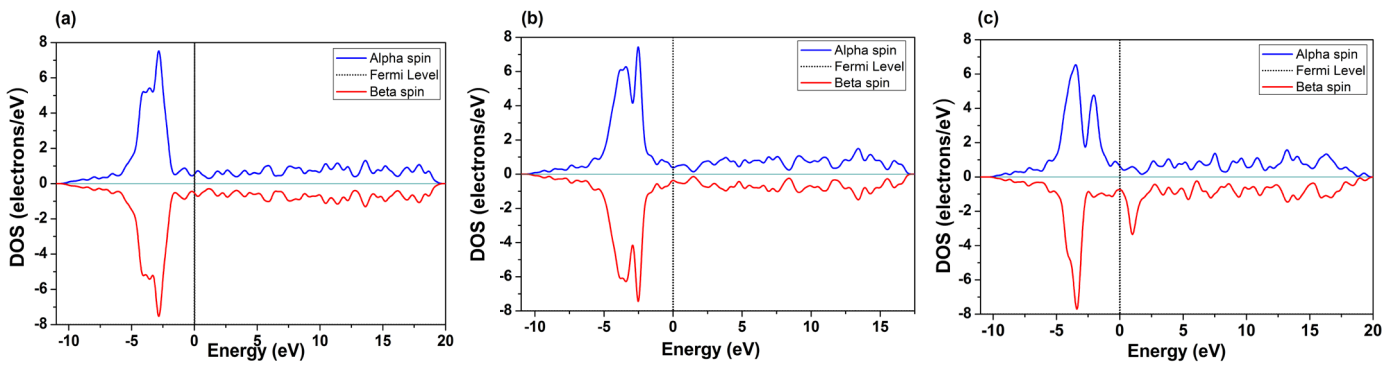
To investigate the magnetic nature of all Cu<sub>(3-x)</sub>Mn<sub>x</sub>Al ( $x = 0, 1$ ) IMCs, the spin polarizability, and total and partial magnetic moments were calculated and compared with each other and presented in Fig. 6. The figures reveal that the minority and majority spin states of the (a) L1<sub>2</sub> and (b) D0<sub>3</sub> type structures exhibit symmetry, indicating the absence of magnetic behavior and polarizability in these structures. In contrast, the (c) L2<sub>1</sub> type structure, which contains Mn atoms and exhibits a Heusler orientation, displays asymmetry between the major and minor spin states, resulting in an asymmetric DOS for the Cu<sub>2</sub>MnAl Heusler alloy.

TABLE 3 lists the partial and total magnetic moments of all type structures. From this table, it is clear that Cu and Al don't have any contribution to magnetization in L1<sub>2</sub> and D0<sub>3</sub> type struc-

TABLE 2

Atomic Mulliken charge &amp; bond populations for all phases

| Compound                  | Type Structure  | Species         | <i>s</i> | <i>p</i> | <i>d</i> | total | Charge (e) | Bond                               | Population |
|---------------------------|-----------------|-----------------|----------|----------|----------|-------|------------|------------------------------------|------------|
| <b>Cu<sub>3</sub>Al</b>   | L1 <sub>2</sub> | Al              | 0.77     | 1.76     | —        | 2.53  | 0.47       | Al-Cu Cu-Cu                        | 0.82       |
|                           |                 | Cu <sub>1</sub> | 0.54     | 0.90     | 9.72     | 11.16 | -0.16      |                                    |            |
|                           |                 | Cu <sub>2</sub> | 0.54     | 0.90     | 9.72     | 11.16 | -0.16      |                                    |            |
|                           |                 | Cu <sub>3</sub> | 0.54     | 0.90     | 9.72     | 11.16 | -0.16      |                                    |            |
|                           | D0 <sub>3</sub> | Al              | 0.78     | 1.74     | —        | 2.51  | 0.49       | Al-Cu <sub>1</sub>                 | 0.70       |
|                           |                 | Cu <sub>1</sub> | 0.44     | 0.79     | 9.72     | 10.94 | 0.06       | Al-Cu <sub>2,3</sub>               | 0.99       |
|                           |                 | Cu <sub>2</sub> | 0.53     | 1.01     | 9.73     | 11.27 | -0.27      | Cu <sub>1</sub> -Cu <sub>2,3</sub> | 0.35       |
|                           |                 | Cu <sub>3</sub> | 0.53     | 1.01     | 9.73     | 11.27 | -0.27      | Cu <sub>2</sub> -Cu <sub>3</sub>   | 0.35       |
| <b>Cu<sub>2</sub>MnAl</b> | L2 <sub>1</sub> | Al              | 0.79     | 1.87     | —        | 2.65  | 0.35       | Al-Mn                              | 0.38       |
|                           |                 | Mn              | 0.13     | 0.26     | 5.64     | 6.02  | 0.98       | Mn-Cu <sub>1,2</sub>               | 0.16       |
|                           |                 | Cu <sub>1</sub> | 0.69     | 1.26     | 9.71     | 11.66 | -0.66      | Al-Cu <sub>1,2</sub>               | 1.19       |
|                           |                 | Cu <sub>2</sub> | 0.69     | 1.26     | 9.71     | 11.66 | -0.66      | Cu <sub>1</sub> -Cu <sub>2</sub>   | 0.42       |

Fig. 6. Spin polarizability for major and minor spin for (a) L1<sub>2</sub> type structure; (b) D0<sub>3</sub> type structure; (c) L2<sub>1</sub> type structure

tures, implying that Cu and Al are nearly non-ferromagnetic due to their equal *Alpha* (*Up*) and *Beta* (*Down*) spin density. In the case of L2<sub>1</sub> type structure, Cu and Al have a small contribution of magnetic moment  $-0.17$  and  $-0.4 \mu_B$  respectively. The presence of the unoccupied minority spin states, identified as Mn *3d* states,

causes the exclusions of electrons with minority spin, leading to the localized moment of Mn *3d*. As a result, the local magnetic moment of Mn is found to be  $3.87 \mu_B$  independently, indicating increased magnetization of the corresponding compound, which is the basic characteristic of Heusler alloys. Our calculated total

TABLE 3

Calculated partial and total magnetic moment of Cu<sub>(3-x)</sub>Mn<sub>x</sub>Al (*x* = 0, 1) in  $\mu_B$  unit

| Compound                  | Type Structure  | Species      | <i>Alpha</i> | <i>Beta</i> | Partial, $\mu_B$ | Total, $\mu_B$   | Ref.   |
|---------------------------|-----------------|--------------|--------------|-------------|------------------|--|--|
| <b>Cu<sub>3</sub>Al</b>   | L1 <sub>2</sub> | Al           | 1.20         | 1.20        | 0                | 0  | —  |
|                           |                 | Cu           | 16.3         | 16.3        | 0                |  |  |
|                           |                 | Sum          | 17.50        | 17.50       | —                |  |  |
|                           |                 | Interstitial | —            | —           | —                |  |  |
|                           | D0 <sub>3</sub> | Al           | 1.22         | 1.22        | 0                | 0  | —  |
|                           |                 | Cu           | 16.3         | 16.3        | 0                |  |  |
|                           |                 | Sum          | 17.52        | 17.52       | —                |  |  |
|                           |                 | Interstitial | —            | —           | —                |  |  |
| <b>Cu<sub>2</sub>MnAl</b> | L2 <sub>1</sub> | Al           | 1.2          | 1.37        | -0.17            | 3.4<br>3.6<br>3.6<br>3.2<br>3.7<br>4<br>3.502<br>3.47<br>3.6<br>3.50 | <b>This work</b><br>Exp. [56]<br>Exp. [57]<br>Exp. (298 K) [58]<br>Exp. (77K) [58]<br>Exp. (4K) [59]<br>Calc. [42]<br>Calc. [52]<br>Calc. [60]<br>Calc. [61] |
|                           |                 | Mn           | 4.96         | 1.09        | 3.87             |  |  |
|                           |                 | Cu           | 11.1         | 11.5        | -0.4             |  |  |
|                           |                 | Sum          | 17.26        | 13.96       | —                |  |  |
|                           |                 | Interstitial | —            | —           | 0.1              |  |  |

magnetic moment of Cu<sub>2</sub>MnAl is in excellent agreement with both the experimental values reported by H. Okumura et al. and the theoretical values obtained by Kulkova et al. as well as other researchers [42,52,56-61].

#### 4. Conclusions

In conclusion, the first-principles calculations based on GGA approximations were used to predict the structural parameters, electronic properties, charge density distribution, and spin polarizability of the Cu<sub>(3-x)</sub>Mn<sub>x</sub>Al ( $x = 0, 1$ ) IMCs. Our results show that the lattice constants are in excellent agreement with experimental and theoretical values reported in the literature. Notably, this study provides the first prediction and discussion of the physical properties of Cu<sub>3</sub>Al with the space group D0<sub>3</sub> (*225-Fm3m*) for the targeted properties. The analysis of the electronic band structures and density of states shows that Cu<sub>3</sub>Al IMCs are metallic and conductive compounds. Furthermore, our findings confirm that Cu<sub>2</sub>MnAl Heusler alloy is a ferromagnetic and metallic compound by nature. Charge density distribution shows the dominant bonding type of each IMC and, demonstrating that the interior bonding of metallic alloys can include a complex interplay of metallic, ionic, and covalent bonding.

#### Acknowledgment

I would like to extend my sincerest appreciation to Prof. Dr. Yusuf ATALAY for his insightful and valuable contributions during the preparation and refinement of this study.

#### REFERENCES

- [1] T. Tian, X.F. Wang, W. Li, Ab initio calculations on elastic properties in L12 structure Al3X and X3Al-type (X=transition or main group metal) intermetallic compounds. *Solid State Commun* **156**, 69-75 (2013). DOI: <https://doi.org/10.1016/j.ssc.2012.10.021>
- [2] R.W. Cahn, Combining metals and sciences: Ways of investigating intermetallics. *Intermetallics (Barking)* **6**, 7-8, 563-566 (1998). DOI: [https://doi.org/10.1016/s0966-9795\(98\)00027-2](https://doi.org/10.1016/s0966-9795(98)00027-2)
- [3] S. Javaheri, M. Babaeipour, A. Boochani, S. Naderi, Electronic and optical properties of V doped AlN nanosheet: DFT calculations. *Chinese Journal of Physics* **56**, 6, 2698-2709 (2018). DOI: <https://doi.org/10.1016/j.cjph.2018.10.021>
- [4] F. Lanzini, P.H. Gargano, P.R. Alonso, G.H. Rubiolo, First-principles study of atomic ordering in bcc Cu-Al. *Model Simul. Mat. Sci. Eng.* **19**, 1 (2011). DOI: <https://doi.org/10.1088/0965-0393/19/1/015008>
- [5] F. Apostol, Y. Mishin, Interatomic potential for the Al-Cu system. *Phys. Rev. B Condens. Matter. Mater. Phys.* **83**, 5, 1-8 (2011). DOI: <https://doi.org/10.1103/PhysRevB.83.054116>
- [6] Y. Liu, J. Wang, Q. Nan Gao, Y. Du, Structural, elastic and electronic properties of Cu-X compounds from first-principles calculations. *J. Cent. South Univ.* **22**, 5, 1585-1594 (2015). DOI: <https://doi.org/10.1007/s11771-015-2675-7>
- [7] W.J. Meng, J. Faber, P.R. Okamoto, L.E. Rehn, B.J. Kestel, R.L. Hitterman, Neutron diffraction and transmission electron microscopy study of hydrogen-induced phase transformations in Zr3Al. *J. Appl. Phys.* **67**, 3, 1312-1319 (1990). DOI: <https://doi.org/10.1063/1.345683>
- [8] N. Boudalia, J.M. Raulot, E. Patoor, C. Esling, Phase Stability Study of the Shape Memory Alloy CuAl-X (X: Be, Zn, Ti, Ni, Ag and Au) by Ab Initio Calculations. *Materials Science Forum* **879**, 250-255 (2017). DOI: <https://doi.org/10.4028/www.scientific.net/MSF.879.250>
- [9] M. Draissia, M.Y. Debili, N. Boukhris, M. Zadam, S. Lallouche, Metastable Ordered Cu3Al Phase in Sputter-Deposited Al-Cu Alloys System. *Copper: Better Properties for Innovative Products*, p. 65-70 (2006). DOI: <https://doi.org/10.1002/9783527610327.ch8>
- [10] F. Heusler, W. Starck, E. Haupt, Magnetisch-chemische studien. *Verh. Dtsch. Phys. Ges.* **5**, 219-232 (1903).
- [11] D.P. Oxley, R.S. Tebble, K.C. Williams, Heusler alloys. *J. Appl. Phys.* **34**, 4, 1362-1364 (1963). DOI: <https://doi.org/10.1063/1.1729511>
- [12] A.N. Titenko, L.D. Demchenko, A.O. Perekos, O.Y. Gerasimov, Effect of Thermomagnetic Treatment on Structure and Properties of Cu-Al-Mn Alloy. *Nanoscale Res. Lett.* **12**, 1 (2017). DOI: <https://doi.org/10.1186/s11671-017-2052-6>
- [13] A. Jazideh, A. Boochani, B. Arghavani Nia, Half-metallic, magneto-optic, and thermoelectric properties of CoRuVZ (Z=Al, Ga). *Phys. Lett. A* **414**, 127622 (2021). DOI: <https://doi.org/10.1016/j.physleta.2021.127622>
- [14] C. Felser, G.H. Fecher, B. Balke, Spintronics: A challenge for materials science and solid-state chemistry. *Angewandte Chemie – International Edition* **46**, 5, 668-699 (2007). DOI: <https://doi.org/10.1002/anie.200601815>
- [15] H. Zabel, Progress in spintronics. *Superlattices Microstruct* **46**, 4, 541-553 (2009). DOI: <https://doi.org/10.1016/j.spmi.2009.07.008>
- [16] X. Wang, Z. Cheng, H. Khachai, R. Khenata, T. Yang, Electronic, magnetic, and thermodynamic properties of rhombohedral Dysprosium Manganite and discussions of effects of uniform strain, spin-orbit coupling, hole and electron doping on its electronic structures. *J. Solid State Chem.* **276**, 352-360 (2019). DOI: <https://doi.org/10.1016/j.jssc.2019.05.030>
- [17] Z. Chen et al., First-Principles Study on a New All- d -Metal Full-Heusler-Based Shape-Memory Alloy Cd2MnPd. *Spin* **9**, 3, 1-7 (2019). DOI: <https://doi.org/10.1142/S2010324719500127>
- [18] R. Bentata et al., New p-type sp-based half-Heusler compounds LiBaX(X=Si, Ge) for spintronics and thermoelectricity via ab-initio calculations. *J. Comput. Electron.* **20**, 3, 1072-1082 (2021). DOI: <https://doi.org/10.1007/s10825-021-01702-x>
- [19] S. Parsamehr et al., Thermodynamic phase diagram and thermoelectric properties of LiMgZ (Z=P, As, Bi): ab initio method study. *Philosophical Magazine* **101**, 3, 369-386, Feb. (2021). DOI: <https://doi.org/10.1080/14786435.2020.1839138>

- [20] V. Milman et al., Electronic Structure, Properties, and Phase Stability of Inorganic Crystals: A Pseudopotential Plane-Wave Study. *Int. J. Quantum Chem.* **77**, 5, 895-910 (2001). DOI: [https://doi.org/10.1002/\(SICI\)1097-461X\(2000\)77:5<895::AID-QUA10>3.0.CO;2-C](https://doi.org/10.1002/(SICI)1097-461X(2000)77:5<895::AID-QUA10>3.0.CO;2-C)
- [21] W. Zhou, L. Liu, B. Li, Q. Song, P. Wu, Structural, elastic, and electronic properties of Al-Cu intermetallics from first-principles calculations. *J. Electron. Mater.* **38**, 2, 356-364 (2009). DOI: <https://doi.org/10.1007/s11664-008-0587-0>
- [22] R. Parvin, F. Parvin, M.S. Ali, A.K.M.A. Islam, Band structure, Fermi surface, elastic, thermodynamic, and optical properties of AlZr<sub>3</sub>, AlCu<sub>3</sub>, and AlCu<sub>2</sub>Zr: First-principles study. *Chinese Physics B* **25**, 8 (2016). DOI: <https://doi.org/10.1088/1674-1056/25/8/083101>
- [23] A. Meng, J. Nie, K. Wei, H. Kang, Z. Liu, Y. Zhao, Optimization of strength, ductility and electrical conductivity of a Cu–Cr–Zr alloy by cold rolling and aging treatment. *Vacuum* **167**, June, 329-335 (2019). DOI: <https://doi.org/10.1016/j.vacuum.2019.06.027>
- [24] N. Ponweiser, C.L. Lengauer, K.W. Richter, Re-investigation of phase equilibria in the system Al-Cu and structural analysis of the high-temperature phase  $\eta$ 1-Al<sub>1</sub>- $\delta$ Cu. *Intermetallics (Barking)* **19**, 11, 1737-1746 (2011). DOI: <https://doi.org/10.1016/j.intermet.2011.07.007>
- [25] A. Alés, F. Lanzini, Mechanical and thermodynamical properties of  $\beta$  - Cu - Al - Mn alloys along the Cu<sub>3</sub>Al  $\rightarrow$  Cu<sub>2</sub>AlMn compositional line. *Solid State Comm.* **319**, 113980 (2020). DOI: <https://doi.org/10.1016/j.ssc.2020.113980>
- [26] M. Şaşmaz, A. Bayri, Y. Aydoğdu, The Magnetic Behavior and Physical Characterization of Cu–Mn–Al Ferromagnetic Shape Memory Alloy. *J. Supercond. Nov. Magn.* **24**, 1, 757-762 (2011). DOI: <https://doi.org/10.1007/s10948-010-0934-2>
- [27] A. Alés, Study of different structures derives of  $\beta$ -Cu<sub>3</sub>Al by means of ab-initio calculations and Quasi-Harmonic Approximation. *Computational Condensed Matter* **31**, e00652 (2022). DOI: <https://doi.org/10.1016/j.cocom.2022.e00652>
- [28] R. Nityananda, P. Hohenberg, W. Kohn, Inhomogeneous electron gas. *Resonance* **22**, 8, 809-811 (2017). DOI: <https://doi.org/10.1007/s12045-017-0529-3>
- [29] W. Kohn, L.J. Sham, Self-consistent equations including exchange and correlation effects. *Physical Review* **140**, 4A, A1133-A1138 (1965). DOI: <https://doi.org/10.1103/PhysRev.140.A1133>
- [30] S.J. Clark et al., First principles methods using CASTEP. *Zeitschrift fur Kristallographie* **220**, 5-6, 567-570 (2005). DOI: <https://doi.org/10.1524/zkri.220.5.567.65075>
- [31] J.P. Perdew, K. Burke, M. Ernzerhof, Generalized gradient approximation made simple. *Phys. Rev. Lett.* **77**, 18, 3865-3868 (1996). DOI: <https://doi.org/10.1103/PhysRevLett.77.3865>
- [32] A.S. Atalay, B. Derin, M.F. Khanghah, First-principles investigation of optical properties of AlFe<sub>(2-x)</sub>MxB<sub>2</sub> (x= 0–1), (M= Cr, V) intermetallic compounds. *Computational Condensed Matter* **32**, e00731 (2022). DOI: <https://doi.org/10.1016/j.cocom.2022.e00731>
- [33] D. Vanderbilt, Soft self-consistent pseudopotentials in a generalized eigenvalue formalism. *Phys. Rev. B* **41**, 11, 7892 (1990). DOI: <https://doi.org/10.1103/PhysRevB.41.7892>
- [34] J.D. Pack, H.J. Monkhorst, 'special points for Brillouin-zone integrations'-a reply. *Phys. Rev. B* **16**, 4, 1748-1749 (1977). DOI: <https://doi.org/10.1103/PhysRevB.16.1748>
- [35] B.G. Pfrommer, M. Côté, S.G. Louie, M.L. Cohen, Relaxation of Crystals with the Quasi-Newton Method. *J. Comput. Phys.* **131**, 1, 233-240 (1997). DOI: <https://doi.org/10.1006/jcph.1996.5612>
- [36] L. Hao, R. Khenata, X. Wang, T. Yang, Ab Initio Study of the Structural, Electronic, Magnetic, Mechanical and Thermodynamic Properties of Full-Heusler Mn<sub>2</sub>CoGa. *J. Electron. Mater.* **48**, 10, 6222-6230 (2019). DOI: <https://doi.org/10.1007/s11664-019-07417-x>
- [37] X.T. Wang, J.W. Lu, H. Rozale, X.F. Liu, Y.T. Gui, G.D. Liu, Half-metallic state and magnetic properties versus the lattice constant in Zr<sub>2</sub>RhZ (Z= Al, Ga, In) Heusler alloys. arXiv preprint arXiv:1505.00203 (2015). DOI: <https://doi.org/10.48550/arXiv.1505.00203>
- [38] C. Liu, F. Yun, H. Morkoc, Ferromagnetism of ZnO and GaN: a review. *Journal of Materials Science: Materials in Electronics* **16**, 555-597 (2005).
- [39] X. Zhou, H. Cao, Z. Zhou, J. Cao, J. Yu, Structural, electrical and optical properties of InGaZnO<sub>4</sub> and In<sub>29</sub>Sn<sub>30</sub>O<sub>48</sub>: a first-principles study. *J. Comput. Electron.* **16**, 2, 280-286 (2017). DOI: <https://doi.org/10.1007/s10825-017-0977-8>
- [40] J. Soltys, Order–disorder phase transitions in ternary alloys Cu<sub>3</sub>–xMnxAl. *Physica Status Solidi (a)*, **63**, 2, 401-406 (1981). DOI: <https://doi.org/10.1002/pssa.2210630204>
- [41] J.M. Vandenberg, R.A. Hamm, An in situ X-ray study of phase formation in CuAl thin film couples. *Thin Solid Films* **97**, 4, 313-323 (1982). DOI: [https://doi.org/10.1016/0040-6090\(82\)90523-5](https://doi.org/10.1016/0040-6090(82)90523-5)
- [42] B. Benichou, Z. Nabi, B. Bouabdallah, H. Bouchenafa, Structural, elastic, electronic and magnetic properties of quaternary Heusler alloy Cu<sub>2</sub>MnSi<sub>1-x</sub>Al<sub>x</sub> (x = 0 - 1): First-principles study. *Revista Mexicana de Fisica* **64**, 2, 135-140 (2018). DOI: <https://doi.org/10.31349/revmexfis.64.135>
- [43] K. Tanaka, T. Saito, Yasuda, Soft X-Ray Emission Spectra of Aluminium in  $\beta$ -Phase Cu-Ni-Al and Cu-Mn-Al Alloys. *J. Phys. Soc. Jpn.* **52**, 1718-1724 (1983). DOI: <https://doi.org/10.1143/JPSJ.52.1718>
- [44] J. Gui et al., Embedded-atom method study of the effect of the order degree on the lattice parameters of Cu-based shape memory alloys. *Journal of Physics: Condensed Matter* **6**, 24, 4601-4614 (1994). DOI: <https://doi.org/10.1088/0953-8984/6/24/019>
- [45] A.S. Atalay, B. Derin, Mechanical effects of Cr and V substitutions in AlFe<sub>2</sub>B<sub>2</sub> by first-principles calculations. *Comput. Mater. Sci.* **239**, 112960 (2024). DOI: <https://doi.org/10.1016/j.commatsci.2024.112960>
- [46] Y. Zhang, Q. Li, Y. He, ReaxFF Molecular Dynamics Simulation of Hydrostatic and Uniaxial Compression of Nitrate Energetic Materials. *ACS Omega* **5**, 29, 18535-18543 (2020). DOI: <https://doi.org/10.1021/acsomega.0c02829>
- [47] F. Birch, Finite elastic strain of cubic crystals. *Physical Review* **71**, 11, 809-824 (1947). DOI: <https://doi.org/10.1103/PhysRev.71.809>

- [48] F.D. Murnaghan, The Compressibility of Media under Extreme Pressures. *Proceedings of the National Academy of Sciences* **30**, 9, 244-247 (1944). DOI: <https://doi.org/10.1073/pnas.30.9.244>
- [49] Md. M. Hossain, First-principles study on the structural, elastic, electronic and optical properties of LiNbO<sub>3</sub>. *Heliyon* **5**, 4, e01436 (2019). DOI: <https://doi.org/10.1016/j.heliyon.2019.e01436>
- [50] S. Hayat, R.M. Arif Khalil, M.I. Hussain, A.M. Rana, F. Hussain, Ab-initio study of the structural, optoelectronic, magnetic, hydrogen storage properties and mechanical behavior of novel combinations of hydride perovskites LiXH<sub>3</sub> (X=Cr, Fe, Co, & Zn) for hydrogen storage applications. *J. Comput. Electron.* **20**, 6, 2284-2299 (2021). DOI: <https://doi.org/10.1007/s10825-021-01807-3>
- [51] J. Jalilian, Comment on 'study of electronic, magnetic, optical and elastic properties of Cu<sub>2</sub>MnAl a gapless full heusler compound'. *J. Alloys Compd.* **626**, 277-279 (2015). DOI: <https://doi.org/10.1016/j.jallcom.2014.12.039>
- [52] S.E. Kulkova, S.V. Ereemeev, T. Kakeshita, S.S. Kulkov, G.E. Rudenski, The electronic structure and magnetic properties of full- and half-heusler alloys. *Mater. Trans.* **47**, 3, 599-606 (2006). DOI: <https://doi.org/10.2320/matertrans.47.599>
- [53] Y. Tian, W. Zeng, Q.J. Liu, Z.T. Liu, Theoretical Study of the Structural, Electronic, Chemical Bonding and Optical Properties of the A<sub>21</sub> am Orthorhombic SrBi<sub>2</sub>Ta<sub>2</sub>O<sub>9</sub>. *Brazilian Journal of Physics* **48**, 1, 25-30 (2018). DOI: <https://doi.org/10.1007/s13538-017-0544-6>
- [54] R.S. Mulliken, Electronic population analysis on LCAO-MO molecular wave functions. I. *J. Chem. Phys.* **23**, 10, 1833-1840 (1955). DOI: <https://doi.org/10.1063/1.1740588>
- [55] M. Segall, R. Shah, C. Pickard, M. Payne, Population analysis of plane-wave electronic structure calculations of bulk materials. *Phys. Rev. B Condens. Matter. Mater. Phys.* **54**, 23, 16317-16320 (1996). DOI: <https://doi.org/10.1103/PhysRevB.54.16317>
- [56] B. Caroli, A. Blandin, Champs hyperfins dans les alliages d'heusler. *Journal of Physics and Chemistry of Solids* **27**, 3, 503-508 (1966). DOI: [https://doi.org/10.1016/0022-3697\(66\)90193-4](https://doi.org/10.1016/0022-3697(66)90193-4)
- [57] H. Takata, Magnetic Form Factor of Cu<sub>2</sub>MnAl. *J. Physical Soc. Japan* **20**, 9, 1743-1744, Sep. (1965). DOI: <https://doi.org/10.1143/JPSJ.20.1743>
- [58] G.P. Felcher, J.W. Cable, M.K. Wilkinson, The magnetic moment distribution in Cu<sub>2</sub>MnAl. *Journal of Physics and Chemistry of Solids* **24**, 12, 1663-1665 (1963). DOI: [https://doi.org/10.1016/0022-3697\(63\)90112-4](https://doi.org/10.1016/0022-3697(63)90112-4)
- [59] K. Tajima, Y. Ishikawa, P.J. Webster, M.W. Stringfellow, D. Tocchetti, K.R.A. Zeabeck, Spin Waves in a Heusler Alloy Cu<sub>2</sub>MnAl\*. *J. Physical Soc. Japan* **43**, 2, 483-489, Aug. (1977). DOI: <https://doi.org/10.1143/JPSJ.43.483>
- [60] H. Okumura, K. Sato, K. Suzuki, T. Kotani, Electronic Structure and Spin-wave Dispersion of Cu<sub>2</sub>MnAl, Ni<sub>2</sub>MnSn, and Pd<sub>2</sub>MnSn Based on Quasi-particle Self-consistent GW Calculations. *J. Physical Soc. Japan* **89**, 3, 034704 (2020). DOI: <https://doi.org/10.7566/jpsj.89.034704>
- [61] Y. Kurtulus, M. Gilleben, R. Dronskowski, Electronic structure, chemical bonding, and finite-temperature magnetic properties of full heusler alloys. *J. Comput. Chem.* **27**, 1, 90-102 (2006). DOI: <https://doi.org/10.1002/jcc.20308>